JACS
JOURNAL OF THE AMERICAN CHEMICAL SOCIETY

Communication

pubs.acs.org/JACS

Phosphoric Acid Loaded Azo (−N═N−) Based Covalent Organic Framework for Proton Conduction

Suman Chandra,[†,†] Tanay Kundu,[†,†] Sharath Kandambeth,[†] Ravichandar BabaRao,[‡] Yogesh Marathe,[†] Shrikant M. Kunjir,[†] and Rahul Banerjee*[,†]

[†]Physical/Materials Chemistry Division, CSIR-National Chemical Laboratory, Dr. Homi Bhabha Road, Pune 411008, India

[‡]Materials Science and Engineering Division, Commonwealth Scientific and Industrial Research Organization (CSIRO), Clayton, Victoria 3168, Australia

Supporting Information

ABSTRACT: Two new chemically stable functional crystalline covalent organic frameworkds (COFs) (**Tp-Azo** and **Tp-Stb**) were synthesized using the Schiff base reaction between triformylphloroglucinol (**Tp**) and 4,4′-azodianiline (**Azo**) or 4,4′-diaminostilbene (**Stb**), respectively. Both COFs show the expected keto-enamine form, and high stability toward boiling water, strong acidic, and basic media. H_3PO_4 doping in **Tp-Azo** leads to immobilization of the acid within the porous framework, which facilitates proton conduction in both the hydrous ($\sigma = 9.9 \times 10^{-4}$ S cm^{-1}) and anhydrous state ($\sigma = 6.7 \times 10^{-5}$ S cm^{-1}). This report constitutes the first emergence of COFs as proton conducting materials.

Covalent Organic Frameworks (COFs) are 2D or 3D crystalline materials made by linking lighter elements (e.g., B, C, N, O) via covalent bonds in a periodic manner.[1] COFs are synthesized and subsequently crystallized by means of reversible covalent bond formation reactions such as boronic acid trimerization, boronate ester formation, and the Schiff base reaction. Structurally, COFs are closely related to metal−organic frameworks (MOFs),[2] where coordination bonds link metal ions and organic struts. Although COFs have shown excellent promise as semiconductive devices,[3d] sensors,[3e,f] and in gas storage and separation,[3a] proton conductivity in COFs is still unexplored. In recent years, proton conducting materials have spurred tremendous interest among researchers due to their application in fuel cells, sensors, and electronic devices.[4] Nafion based proton conducting membranes are considered as the benchmark in this field. Such membranes exhibit high proton conductivity (ca. 10^{-1} S cm^{-1}) at moderate temperature (60−80 °C) under high relative humidity (98% RH).[4c] Yet, the high cost of perfluorinated membranes with less efficiency at fuel cell operating temperatures (ca. 120 °C) encouraged researchers to search for alternative materials. In this context, MOFs with loaded carrier molecules (e.g., imidazole, triazole, mineral acids) have been envisaged for high temperature proton conduction applications.[5] However, MOFs suffer poor hydrolytic stability with very low pH tolerance of the occluded guests. As a result, rupture of the coordination bonds and the framework backbone limits its applicability in fuel cell operating conditions. In addition, the high gravimetric weight of the MOF, difficulty in forming compact membranes, and instability at higher temperatures are major limitations for the future development of proton conducting materials. COFs are relatively lightweight, exhibit a wide variety of functionality, and possess high thermal stability and membrane processability like polymers. These features ensure their sustainability in harsh fuel cell operating conditions and a high degree of internal ordering as in MOFs that facilitates loading and the transport of proton conducting substrates. Despite these promising features, COFs have never been tested for proton conduction due to their instability[6] in ambient humidity conditions.

We recently overcame this stability problem and developed a general strategy for synthesizing COFs that showcase the stability toward a strong acid (9 N HCl) and moderately strong base (6 N NaOH), even upon isoreticulation and functionalization.[7] Also, the COF backbone can be suitably functionalized, which can further enhance the interaction with carrier molecules to aid proton conduction pathways. H_3PO_4 loaded PBI based membranes are well documented in literature for high proton conductivity (ca. 10^{-2} S cm^{-1}) at fuel cell operating temperatures.[8] Other than the benzimidazole group, the azo group can also play a vital role in stabilizing H_3PO_4.[9] The crystal structure of the protonated azobenzene unit [ref code: WEVXAX][9a] with the H-bonded $H_2PO_4^-$ anion hints at the potential of azo functionalized COFs to act as proton conducting materials. The extension of the azobenzene monomeric unit in higher dimensions to form a porous COF with a 1D channel may facilitate unidirectional proton transport, while crystallinity and chemical stability may be beneficial in providing mechanistic insight. In this regard, we present an azo functionalized COF (**Tp-Azo**) made by the Schiff base reaction between triformylphloroglucinol (**Tp**) and 4,4′-azodianiline (**Azo**). This COF exhibits excellent structural stability, porosity, and crystallinity even after acid treatment. As mentioned before, we conceived this idea of a H_3PO_4 loaded azo functionalized COF (**PA@Tp-Azo**) being a good proton conductor after noticing the crystal structure of H_3PO_4 treated 4-aminoazobenzene, where H_3PO_4 finds an anchoring site at the azo center by protonating it, while the $H_2PO_4^-$ anions are stabilized via H-bonds.[9a] **PA@Tp-Azo** shows proton conductivity in humid and anhydrous conditions (9.9×10^{-4} and 6.7×10^{-5} S cm^{-1}, respectively). To elucidate the structure/property relationship, we also synthesized the nonazo

Received: March 8, 2014
Published: April 23, 2014

   dx.doi.org/10.1021/ja502212v | J. Am. Chem. Soc. 2014, 136, 6570−6573

counterpart, i.e. stilbene functionalized COF (**Tp-Stb**) which shows less stability, crystallinity, porosity, and much less proton conductivity than **Tp-Azo** because of the nonavailability of an anchoring site.

The syntheses of **Tp-Azo** and **Tp-Stb** were done by reacting **Tp** (63 mg, 0.3 mmol) with **Azo** (96 mg, 0.45 mmol) or **Stb** (128 mg, 0.45 mmol) using (1:1) dimethylacetamide and *o*-dichlorobenzene as solvent (3 mL) (Figure 1). The reactants were first

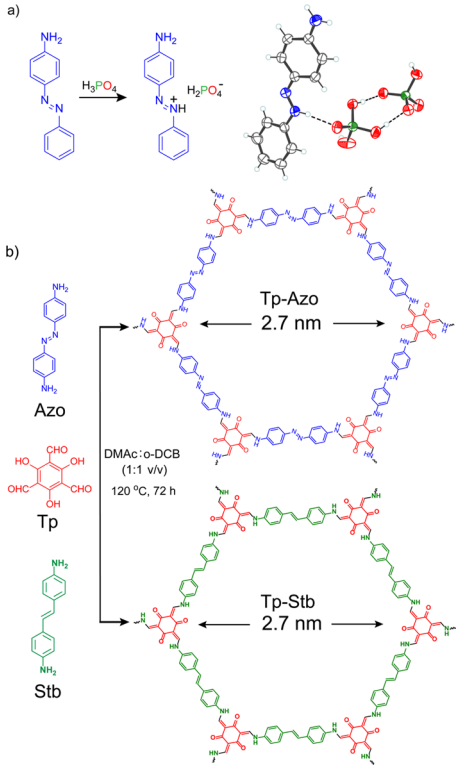

Figure 1. (a) Crystal structure of 4-[(*E*)-phenyl-diazenyl]anilinium dihydrogen phosphate.[9a] (b) Schematic of **Tp-Azo** and **Tp-Stb** synthesis.

dispersed by ultrasonication for 10 min and then degassed through three freeze–pump–thaw cycles. The tubes were then vacuum sealed and placed in an isotherm oven for 3 days at 120 °C. Finally, the material was filtered out and washed with dry acetone and dried under vacuum at 150 °C for 12 h. The PXRD patterns of **Tp-Azo** indicate an intense peak at $2\theta = 3.2°$, which corresponds to 100 plane reflections (Figure 2a), with minor peaks at 5.5°, 6.4°, 8.4°, and 27° (001 plane). The $\pi-\pi$ stacking distance between COF layers was calculated to be 3.3 Å from the *d* spacing between 001 planes. On the other hand, **Tp-Stb** exhibits an intense peak at $2\theta = 3.2°$ followed by a broad peak at 5.5°. A possible 2D model was built with an eclipsed structure in the hexagonal space group ($P6/m$) and a staggered structure in the $P1$ space group, by using the software Crystal 09.[10] The experimental PXRD pattern matches well with the simulated pattern of the eclipsed stacking model (Figures S1 and S3, Supporting Information (SI)). In order to find out the unit cell parameters, Pawley refinements were done for both of the COFs. The unit cell value was found to be ($a = b = 31.5$ Å, $c = 3.3$ Å) for **Tp-Azo** and ($a = b = 30.500$ Å, $c = 3.49$ Å) for **Tp-Stb**. The intensity ratio of the first and second peak in the eclipsed form matches with the PXRD of **Tp-Stb**. The energy calculation of both eclipsed and staggered forms of **Tp-Stb** also suggests an eclipsed stacking model with lower energy (Section S-3, SI).

The FT-IR spectra of **Tp-Azo** and **Tp-Stb** indicate the total consumption of starting materials due to the disappearance of the N–H stretching bands (3100–3300 cm^{-1}) of **Azo** or **Stb** and the carbonyl stretching bands (1639 cm^{-1}) of **Tp** (Figure 2b). The strong peak at 1578 cm^{-1} arises due to the C=C stretching in the keto-form similar to the FT-IR spectrum of the reference compound 2,4,6-tris((phenyldiazenyl)phenylamino-methylene)cyclohexane-1,3,5-trione. Most of the FT-IR peaks of **Tp-Azo** and **Tp-Stb** match well with those of the reference compound (Figure 2b). The C=O peaks (1619 cm^{-1}) of **Tp-Azo** and **Tp-Stb** get merged with the C=C stretching band (1582 cm^{-1}). The isolation of **Tp-Azo** and **Tp-Stb** as the keto-form was confirmed by ^{13}C CP-MAS solid state NMR. Both COFs show carbonyl (C=O) carbon signals at $\delta = 181$ and 186 ppm for **Tp-Azo** and **Tp-Stb** respectively. In the starting material, the trialdehyde carbonyl (C=O) carbon resonates at a downfield position around $\delta = 192$ ppm. The absence of a peak at $\delta = 192$ ppm in the ^{13}C CP-NMR spectrum also indicates the total consumption of the starting materials (Figures 2c and S-8, SI). To investigate the protonation of the azo bond by phosphoric acid in **PA@Tp-Azo**, we have done ^{31}P CP-NMR, which shows two distinct peaks at δ −1.31 ppm and δ −14.3 ppm. The ^{31}P resonance peak at δ −1.31 ppm is attributed to the undissociated H_3PO_4 and the shoulder at δ −14.3 ppm corresponds to the $H_2PO_4^-$ anion, which indicates the protonation of the azo bond. However, in **PA@Tp-Stb**, only a single intense peak at δ −0.88 ppm, corresponding to undissociated H_3PO_4, has been observed and the peak at δ −14.3 ppm was absent. This explains the absence of the $H_2PO_4^-$ anion due to the lack of protonation sites in **Tp-Stb** (Figure 3b).

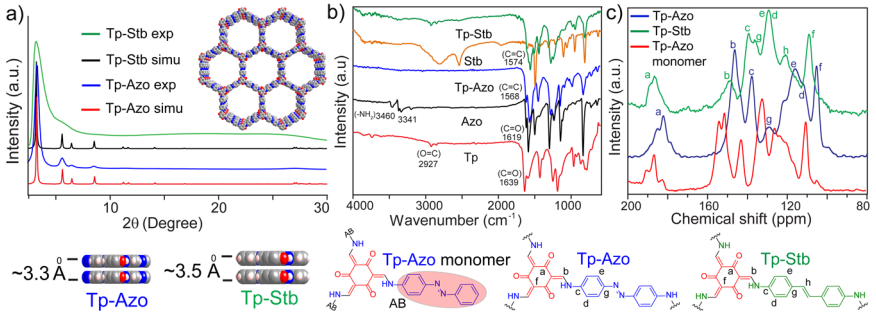

Figure 2. (a) Observed PXRD patterns of **Tp-Azo** (blue) and **Tp-Stb** (green) compared with simulated eclipsed patterns. (b) FT-IR spectra of **Tp-Azo** and **Tp-Stb** compared with starting material **Tp**, **Azo**, and **Stb**. (c) ^{13}C NMR comparison of **Tp-Azo** (blue), **Tp-Stb** (green) against the reference compound **Tp-Azo** monomer = 2,4,6-tris(((4-((*E*)-phenyldiazenyl)phenyl)amino)methylene)cyclohexane-1,3,5-trione (red).

dx.doi.org/10.1021/ja502212v | *J. Am. Chem. Soc.* 2014, 136, 6570–6573

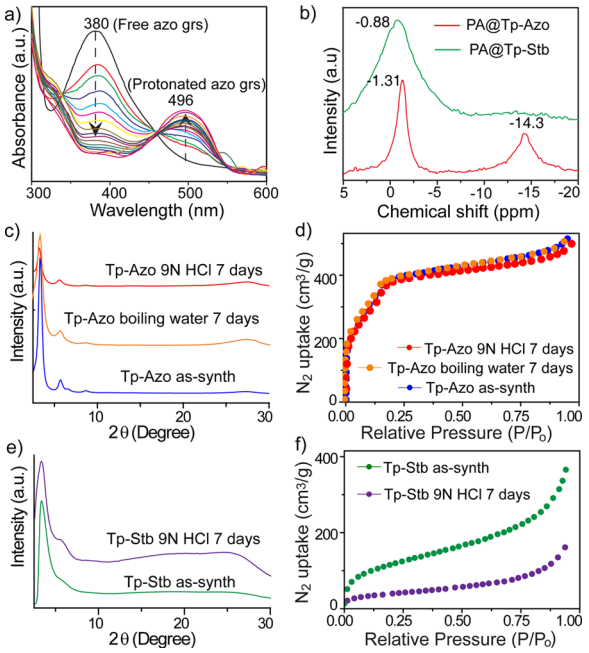

Figure 3. (a) Changes in the UV−vis spectra of monomer of **Tp-Azo** with increasing concentration of H_3PO_4. (b) ^{31}P CP-NMR of H_3PO_4 treated **Tp-Azo** and **Tp-Stb**. (c) PXRD patterns of HCl (red), boiling water (orange) treated and as-synthesized **Tp-Azo** (blue). (d) N_2 adsorption isotherms of **Tp-Azo** (blue), boiling water (orange) and acid treated **Tp-Azo** (red). (e) PXRD patterns of HCl treated (blue) and as-synthesized **Tp-Stb** (green). (f) N_2 adsorption isotherms of as-synthesized **Tp-Stb** (green) and 9 N HCl treated **Tp-Stb** (blue).

SEM and TEM images showed that **Tp-Azo** and **Tp-Stb** crystallize with a flower-like morphology with the aggregation of a large number of petals with an average length of 40−50 nm (Sections S-9 and S-10, SI).

Thermogravimetric analysis (TGA) of the activated **Tp-Azo** and **Tp-Stb** show thermal stability up to 350 °C, with a gradual weight loss of 50% after 360 °C due to the decomposition of the framework (Section S-8, SI). The permanent porosity of **Tp-Azo** and **Tp-Stb** were evaluated by the N_2 adsorption isotherm at 77 K, which showed a reversible type IV adsorption isotherm. The surface areas of the activated COFs, calculated using the BET model, were 1328 and 422 m^2/g for **Tp-Azo** and **Tp-Stb**, respectively (Figure 3d,f). The lower surface area of **Tp-Stb** may be due to the poor crystallinity and not so uniform channels resulting from the lower solubility of **Stb** precursors in organic solvents. The pore size distribution of **Tp-Azo** and **Tp-Stb** shows a narrow distribution of 1.6−2.5 nm (Section S-7, SI).

The stability of **Tp-Azo** and **Tp-Stb** were assayed by immersing 50 mg of COFs in 20 mL of boiling water or by standing in 20 mL strong mineral acids (9 N HCl/1.5 M H_3PO_4) and bases (3−6 N NaOH). Interestingly, both **Tp-Azo** and **Tp-Stb** remain stable, crystalline, and porous while directly submerged in boiling water for several days (7 days), as verified by PXRD, FT-IR spectra, and N_2 adsorption isotherm studies. They also exhibit strong acid (9 N HCl) stability with near retention of molecular crystallinity. However, base treated (3−6 N NaOH) COFs show moderate base stability with partial retention of crystallinity (Figures S20 and S23). The N_2 adsorption isotherm of the 9 N HCl treated **Tp-Azo** indicates the retention of its intrinsic porosity, while **Tp-Stb** shows a decrease in porosity after the acid treatment. However, 1.5 M H_3PO_4 treatment shows a significant loss of porosity in both cases (Figure S9, SI), which is indicative of H_3PO_4 loading. The protonation of the −N═N− functionality in 4-aminoazobenzene[9a] by H_3PO_4 and the well established phenomena of color change of methyl orange in acidic medium[9b] suggested to us that azo-groups are susceptible to protonation and can stabilize counteranions such as phosphate or dihydrogen phosphate. Moreover, H_3PO_4 exhibits high proton conductivity (10^{-1} S cm^{-1}) due to low volatility (>158 °C) and high proton mobility resulted from the extended H-bonding utilizing three ionizable O−H bonds. So we decided to apply this concept in COFs for the synthesis of azo based proton conducting COFs. H_3PO_4 loading in **Tp-Azo** and **Tp-Stb** was achieved by simply immersing the evacuated COF materials in 1.5 M H_3PO_4 for 2 h. Further washing with a copious amount of water (×2) followed by activating overnight at 353 K under dynamic vacuum lead to H_3PO_4 loaded **PA@Tp-Azo** and **PA@Tp-Stb** (Figure 4a). It is noteworthy that the H_3PO_4 loaded COFs exhibit

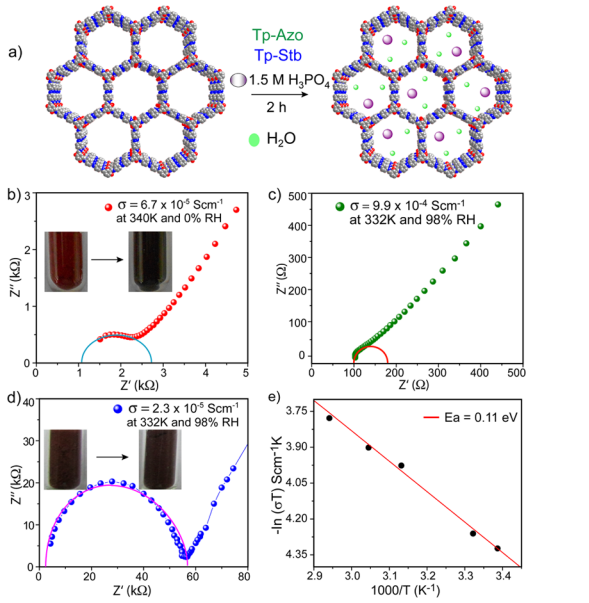

Figure 4. (a) Schematic of H_3PO_4 doping in COFs. Proton conductivity of **PA@Tp-Azo** in (b) anhydrous and (c) hydrous conditions. (d) Proton conductivity of **PA@Tp-Stb** in hydrous conditions. (e) Arrhenius plot for **PA@Tp-Azo** in hydrous conditions.

identical IR spectra and ^{13}C NMR spectra along with moderate crystallinity and porosity compared to the parent COFs (Figures S7 and S21). **Tp-Azo** possesses a higher acid loading (5.4 wt %) as compared to **Tp-Stb** (2.8 wt %), which is evident from the TGA analysis. The proton conductivities of **Tp-Azo**, **Tp-Stb**, **PA@Tp-Azo**, and **PA@Tp-Stb** were measured in both hydrous and anhydrous conditions. The conductivities were determined from the semicircles in the Nyquist plots (Figure 4b−d). Interestingly, both **Tp-Azo** and **Tp-Stb** exhibit almost zero conductivity, which signifies that the COF backbones are acting as a support. The proton conductivity of **PA@Tp-Azo** and **PA@Tp-Stb** were measured from 295 to 415 K. Conductivity values gradually increase upon heating, which reaches a maximum at a temperature of ca. 332−340 K and then decreases gradually upon increasing the temperature. The proton conductivity of **PA@Tp-Azo** was measured as 6.7×10^{-5} S cm^{-1} at 340 K under anhydrous conditions. This value was highly humidity-dependent and increased upon humidification. Finally, **PA@Tp-Azo** exhibited a proton conductivity of 9.9×10^{-4} S cm^{-1} at 332 K

dx.doi.org/10.1021/ja502212v | J. Am. Chem. Soc. 2014, 136, 6570−6573

under 98% relative humidity (RH) (Section S-13, SI). The proton conductivity of **PA@Tp-Azo** is lower than that of its MOF counterparts, i.e. ferrous oxalate dihydrate[5e] (1.3×10^{-3} S cm $^{-1}$ at 298 K, 98% RH) and 1,2,4-triazole loaded β-PCMOF2 (5×10^{-4} S cm^{-1} at 423 K, 20% RH) (full comparison in Table S3 in SI). Surprisingly, **PA@Tp-Stb** shows almost zero proton conductivity in anhydrous conditions, while exhibiting a poor proton conductivity value of 2.3×10^{-5} S cm^{-1} at 332 K under 98% RH. Notably, **PA@Tp-Azo** exhibited an activation energy value of 0.11 eV (Figure 4e), which is much lower than that of Nafion (0.22 eV) and its MOF counterparts (Table S3, SI) operating under humid conditions. Clearly, **PA@Tp-Azo** and **PA@Tp-Stb** show distinct proton conductivity behavior under similar conditions, although they are treated with the same amount of H_3PO_4. Nevertheless, **Tp-Azo** exhibits a distinct color change (red to black) upon H_3PO_4 treatment, while the color of **Tp-Stb** remains almost unchanged (gray). The UV−vis spectra of the H_3PO_4 treated **Tp-Azo** monomer are red-shifted from 380 to 496 nm due to the protonation of the azo bond (Figures S25 and S26). However, the −NH− and the −C═C− groups remain unaffected after acid treatment, which can be proved from the intact UV−vis spectra of 2,4,6-tris(([1,1′-biphenyl]-4-ylamino)-methylene)cyclohexane-1,3,5-trione (monomer of **TpBD**) and stillbene. These observations hint at the interaction between the proton responsive azo group and H_3PO_4, which is the governing factor for the high proton conductivity value of **PA@Tp-Azo** in both humid and anhydrous conditions, a mechanism absent in **PA@Tp-Stb**. We anticipate that the loaded H_3PO_4 along with adsorbed water molecules get H-bonded with the protonated azo groups stacked along the crystallographic *a* axis, which conduct the proton through the framework.

In summary, we for the first time have reported azo and alkene functionalized COFs (**Tp-Azo** and **Tp-Stb**) as proton conducting materials. Exceptional chemical stability, low density, and high thermal stability make them advantageous over their MOF counterparts. We have demonstrated a simple impregnation strategy to load mineral acid viz. H_3PO_4 inside the framework. Interestingly, after the acid treated samples are washed, the COFs retain their crystallinity, porosity, and stability, which make them attractive for proton conduction applications. While the parent COFs exhibit negligible conductivity, **PA@Tp-Azo** shows decent proton conductivity values under both hydrous and anhydrous conditions. **PA@Tp-Stb**, on the other hand, exhibits poor proton conductivity and, that too, only under hydrous conditions. Thus, minute changes in functionality lead to a drastic change in proton conducting ability, which establishes the crucial role of the proton responsive azo group in facilitating proton conduction pathways. Although 2D COFs lack long-range ordering in bulk solid and generate a grain boundary (like MOFs) which may decrease proton conductivity, 3D COFs[11] with the azo group (−N═N−) acting as a phosphoric acid anchoring site could prove advantageous in the long run. In addition, the membrane compatibility of COFs may be beneficial toward the preparation of COF−polymer composites, an ongoing effort in our laboratory. We believe that our findings will encourage further work in COF based functional proton conducting materials in the near future.

■ ASSOCIATED CONTENT

Ⓢ Supporting Information

Synthetic procedures, PXRD, ^{13}C solid state NMR, TGA, UV, crystallographic data (CIF). This material is available free of charge via the Internet at http://pubs.acs.org.

■ AUTHOR INFORMATION

Corresponding Author

r.banerjee@ncl.res.in

Author Contributions

†S.C. and T.K. contributed equally.

Notes

The authors declare no competing financial interest.

■ ACKNOWLEDGMENTS

S.C. and T.K. acknowledge UGC and CSIR (New Delhi, India) for JRF and SRF. R.B. acknowledges [CSC0122 and CSC0102] and DST (SB/SI/IC-32/2013) for funding. We acknowledge Dr. T. G. Ajithkumar, Dr. K. Sreekumar, and Dr. C. Ramesh for NMR, Proton Conduction, and PXRD facilities.

■ REFERENCES

(1) (a) Côté, A. P.; Benin, A. I.; Ockwig, N. W.; Matzger, A. J.; O'Keeffe, M.; Yaghi, O. M. *Science* **2005**, *310*, 1166. (b) Feng, X.; Ding, X.; Jiang, D. *Chem. Soc. Rev.* **2012**, *41*, 6010. (c) Colson, J. W.; Dichtel, W. R. *Nat. Chem.* **2013**, *5*, 453.

(2) (a) Janiak, C. *Dalton Trans.* **2003**, 2781. (b) O'Keeffe, M.; Yaghi, O. M. *Chem. Rev.* **2012**, *112*, 675. (c) Zhou, H. C.; Long, J. R.; Yaghi, O. M. *Chem. Rev.* **2012**, *112*, 673. (d) Furukawa, H.; Cordova, K. E.; O'Keeffe, M.; Yaghi, O. M. *Science* **2013**, *341*, 6149.

(3) (a) Han, S. S.; Furukawa, H.; Yaghi, O. M.; Goddard, W. A. *J. Am. Chem. Soc.* **2008**, *130*, 11580. (b) Furukawa, H.; Yaghi, O. M. *J. Am. Chem. Soc.* **2009**, *131*, 8875. (c) Rabbani, M. G.; Sekizkardes, A. K.; Kahveci, Z.; Reich, T. E.; Ding, R.; El-Kaderi, H. M. *Chem.—Eur. J.* **2013**, *19*, 3324. (d) Wan, S.; Guo, J.; Kim, J.; Ihee, H.; Jiang, D. *Angew. Chem., Int. Ed.* **2008**, *120*, 8958. (e) Dogru, M.; Handloser, M.; Auras, F.; Kunz, T.; Medina, D.; Hartschuh, A.; Knochel, P.; Bein, T. *Angew. Chem.* **2013**, *52*, 2920. (f) Gopalakrishnan, D.; Dichtel, W. R. *J. Am. Chem. Soc.* **2013**, *135*, 8357.

(4) (a) Mauritz, K. A.; Moore, R. B. *Chem. Rev.* **2004**, *104*, 4535. (b) Hickner, M.; Ghassemi, H.; Kim, Y. S.; Einsla, B. R.; McGrath, J. E. *Chem. Rev.* **2004**, *104*, 4587. (c) Paddison, S. J. *Annu. Rev. Mater. Res.* **2003**, *33*, 289.

(5) (a) Ponomareva, V. G.; Kovalenko, K. A.; Chupakhin, A. P.; Dybtsev, D. N.; Shutova, E. S.; Fedin, V. P. *J. Am. Chem. Soc.* **2012**, *134*, 15640. (b) Bureekaew, S.; Horike, S.; Higuchi, M.; Mizuno, M.; Kawamura, T.; Tanaka, D.; Yanai, N.; Kitagawa, S. *Nat. Mater.* **2009**, *8*, 831. (c) Hurd, J. A.; Vaidhyanathan, R.; Thangadurai, V.; Ratcliffe, C. I.; Moudra-kovski, I. M.; Shimizu, G. K. H. *Nat. Chem.* **2009**, *1*, 705. (d) Yoon, M.; Suh, K.; Kim, H.; Kim, Y.; Selvapalam, N.; Kim, K. *Angew. Chem., Int. Ed.* **2011**, *50*, 7870. (e) Yamada, T.; Sadakiyo, M.; Kitagawa, H. *J. Am. Chem. Soc.* **2009**, *131*, 3144.

(6) (a) Lanni, L. M.; Tilford, R. W.; Bharathy, M.; Lavigne, J. J. *J. Am. Chem. Soc.* **2011**, *130*, 11872.

(7) (a) Kandambeth, S.; Mallick, A.; Lukose, B.; Mane, V. M.; Heine, T.; Banerjee, R. *J. Am. Chem. Soc.* **2012**, *134*, 19524. (b) Biswal, B. P.; Chandra, S.; Kandambeth, S.; Lukose, B.; Mane, V. M.; Heine, T.; Banerjee, R. *J. Am. Chem. Soc.* **2013**, *135*, 5328. (c) Chandra, S.; Kandambeth, S.; Biswal, B. P.; Lukose, B.; Kunjir, S. M.; Chaudhary, M.; Babarao, R.; Heine, T.; Banerjee, R. *J. Am. Chem. Soc.* **2013**, *135*, 17853.

(8) Asensio, J. A.; Sanchez, E. M.; Gomez-Romero, P. *Chem. Soc. Rev.* **2010**, *39*, 3210.

(9) (a) Halasz, I.; Lukic, K.; Vancik, H. *Acta Crystallogr.* **2007**, *C63*, o61. (b) Sanchez, A. M.; Barra, M.; de Rossi, R. H. *J. Org. Chem.* **1999**, *64*, 1604.

(10) Dovesi, R.; Saunders, V. R.; Roetti, C.; Orlando, R.; ZicovichWilson, C. M.; Pascale, F.; Civalleri, B.; Doll, K.; Harrison, N. M.; Bush, I. J.; Arco, P. D.; Llunell, M. *Crystal* 1.0.2 ed.

(11) Beaudoin, D.; Maris, T.; Wuest, J. D. *Nat. Chem.* **2013**, *5*, 830.